

Generalized Nagaoka ferromagnetism accompanied by flavor-selective Mott states in an $SU(N)$ Fermi-Hubbard model

Juntaro Fujii,* Kazuki Yamamoto, and Akihisa Koga

Department of Physics, Institute of Science Tokyo, Meguro, Tokyo 152-8551, Japan

(Dated: December 2, 2025)

We study the ferromagnetic instability in an $SU(N)$ Fermi-Hubbard model on the hypercubic lattice. Combining dynamical mean-field theory with continuous-time quantum Monte Carlo simulations, we find that, in the strong-coupling regime at low temperatures, ferromagnetically ordered (FM) states develop away from the commensurate fillings. In the particle-doped $SU(3)$ system near one-third filling, the FM state is accompanied by a spontaneous flavor-selective Mott state, where two of the three flavors are Mott insulating while the remaining flavor is metallic. Since particles in the metallic flavor can almost freely move on the lattice without correlation effects, the ordered state is stabilized by the kinetic-energy gain of the doped particles. This is similar to the generalized Nagaoka ferromagnetism discussed in the one-hole-doped system at one-third filling. In the $SU(4)$ case, we find that six distinct types of FM states appear as the particle density varies. The results uncover the nature of the FM state in the $SU(N)$ Fermi-Hubbard systems and highlight the rich magnetic behavior enabled by enlarged internal symmetries.

I. INTRODUCTION

Recent experimental progress with ultracold atoms has enabled the exploration of strongly correlated quantum phenomena [1–8], by utilizing Feshbach resonances [9] and optical lattices [10]. Fermionic systems with multiple internal states have been realized by exploiting the hyperfine states such as in ^{40}K [11], ^6Li [12–14], ^{173}Yb [15–18], ^{171}Yb [16], and ^{87}Sr [19, 20]. While $SU(2)$ systems have been extensively investigated, these multicomponent atomic gases now enable the study of $SU(N)$ Fermi-Hubbard models with $N > 2$ [21, 22], where the metal-insulator crossover [23] and anti-ferromagnetic correlations [24, 25] have been observed. Generalizing strongly correlated phenomena to those with $SU(N)$ symmetry has opened up new possibilities for understanding exotic quantum phases in condensed matter physics [26–36].

Ferromagnetism in correlated electron systems has long been a central topic in condensed matter physics. The ferromagnetically ordered (FM) states are often realized in realistic multiband systems, originating from the ferromagnetic exchange mechanisms such as Hund’s coupling and double exchange. By contrast, it is not trivial whether the FM state can emerge in the Fermi-Hubbard model without explicit magnetic exchange interactions. In the weak-coupling regime, Slater-type ferromagnetism has been discussed, although its applicability is limited [37]. Flat-band ferromagnetism has also been studied as another route toward itinerant magnetism [38, 39]. However, few theoretical approaches are available in the strong-coupling regime, and systematic understanding remains limited. A prominent exception is Nagaoka ferromagnetism, which is rigorously established for the single-hole-doped $SU(2)$ Fermi-Hubbard model at half filling [40]. Its extensions to finite hole doping, finite temperatures, and higher symmetries such as $SU(N)$ have been discussed by numerical calculations [41–48] as well as analytical studies [49–52]. In our previous work [45], by means of

numerically reliable methods, we clarified that an FM state characterized by the generalized Nagaoka ferromagnetism emerges in the $SU(3)$ Fermi-Hubbard model when holes are doped away from one-third filling. In general, for $N > 2$, the internal flavor degrees of freedom introduce many competing configurations even at commensurate fillings [53], and the kinetic-energy-driven mechanism underlying Nagaoka ferromagnetism does not directly carry over. It still remains unclear whether FM phases can emerge around commensurate fillings in $SU(N)$ systems beyond the Nagaoka mechanism. Therefore, detailed numerical investigations are essential for clarifying the ferromagnetic instability in the $SU(N)$ Fermi-Hubbard model.

In this paper, we investigate the ferromagnetic instability in the $SU(N)$ Fermi-Hubbard model on the hypercubic lattice, using dynamical mean field theory (DMFT) [54–56]. In the $SU(3)$ case, we demonstrate that, in addition to the well-known FM state, which is adiabatically connected to the generalized Nagaoka ferromagnetism, another FM phase emerges together with a spontaneous flavor-selective Mott state above one-third filling, where two of the three flavors are Mott insulating and the other is metallic. For the $SU(4)$ case, six distinct types of FM states are realized away from the commensurate fillings. These results highlight how increasing the number of internal components qualitatively enriches the magnetic phase structure. The ferromagnetic instability in the $SU(N)$ Fermi-Hubbard model is also addressed.

The rest of this paper is organized as follows. In Sec. II, we introduce the $SU(N)$ Fermi-Hubbard model and briefly describe the DMFT framework. In Sec. III, we clarify that, in the strong-coupling regime at low temperatures, the FM states are stabilized in the $SU(3)$ and $SU(4)$ Fermi-Hubbard models. The ferromagnetic instability in the $SU(N)$ case is discussed. Conclusions are given in Sec. IV.

* fujii.j.47dc@m.isct.ac.jp

II. METHODS

We consider the $SU(N)$ Fermi-Hubbard model on a hypercubic lattice, which is described by the Hamiltonian as

$$\hat{H} = -t \sum_{\langle i,j \rangle} \sum_{\sigma=1}^N \hat{c}_{i,\sigma}^\dagger \hat{c}_{j,\sigma} + \frac{U}{2} \sum_i \sum_{\sigma \neq \sigma'} \hat{n}_{i,\sigma} \hat{n}_{i,\sigma'}, \quad (1)$$

where $\hat{c}_{i,\sigma}^\dagger$ ($\hat{c}_{i,\sigma}$) is the creation (annihilation) operator of a fermion with flavor σ ($= 1, 2, \dots, N$) at site i , and $\hat{n}_{i,\sigma} = \hat{c}_{i,\sigma}^\dagger \hat{c}_{i,\sigma}$. t is the hopping amplitude between nearest-neighbor site pair $\langle i, j \rangle$ and U is the on-site repulsive interaction. We employ the grand canonical ensemble, in which the expectation value of an operator \hat{A} is given by $\langle \hat{A} \rangle = \text{Tr} [e^{-(\hat{H} - \mu \hat{N})/T} \hat{A}] / Z$, where μ is the chemical potential, T is the temperature, $Z = \text{Tr} [e^{-(\hat{H} - \mu \hat{N})/T}]$, and $\hat{N} = \sum_{i,\sigma} \hat{n}_{i,\sigma}$. The particle density of each flavor is defined by $n_\sigma = \sum_i \langle \hat{n}_{i,\sigma} \rangle / L$, where L is the number of lattice sites. The total number of particles is represented by $n_{\text{tot}} = \sum_\sigma n_\sigma$. Since the model is particle-hole symmetric, we focus on the filling range $0 \leq n_{\text{tot}} \leq N/2$.

To study low-temperature properties in the $SU(N)$ Fermi-Hubbard model, we employ DMFT [54–56]. In DMFT, the original lattice model is mapped to a single-impurity model coupled to an effective bath. It is known that, in the limit of infinite spatial dimensions, DMFT is exact [56], as it correctly captures local dynamical correlations. DMFT has been successfully applied to analyze various strongly correlated phenomena such as the Mott transition [57–63], superconductivity [64–71], and magnetic ordering [72–75].

The FM state we focus on in this study is, in general, characterized by the order parameter $m_\alpha = \langle \hat{S}_\alpha \rangle / L$ with

$$\hat{S}_\alpha = \frac{1}{2} \sum_{i,\sigma,\sigma'} \hat{c}_{i,\sigma}^\dagger (\lambda_\alpha)_{\sigma,\sigma'} \hat{c}_{i,\sigma'}, \quad (2)$$

where λ_α are the α ($= 1, \dots, N^2 - 1$)th generator of $SU(N)$ with $\text{Tr}[\lambda_\alpha \lambda_\beta] = 2\delta_{\alpha,\beta}$ [76, 77]. Since an imbalance among the flavor occupations serves as a reliable indicator of ferromagnetic order, it is sufficient to characterize the magnetic order using the $(N - 1)$ diagonal generators, whose matrix elements have vanishing off-diagonal components. Consequently, one can restrict the analysis to the diagonal components of Green's function without loss of generality.

The Dyson equation for the lattice Green's function is then given by

$$G^\sigma(k, i\omega_n)^{-1} = i\omega_n + \mu - \epsilon_k - \Sigma^\sigma(k, i\omega_n), \quad (3)$$

where ϵ_k denotes the dispersion relation, $\omega_n [= (2n + 1)\pi T]$ is the Matsubara frequency, and $G^\sigma(k, i\omega_n)$ and $\Sigma^\sigma(k, i\omega_n)$ represent the lattice Green's function and the self-energy with flavor σ . In infinite dimensions, the self-energy is momentum-independent, $\Sigma_{\text{loc}}^\sigma(i\omega_n) = \Sigma^\sigma(k, i\omega_n)$, and the local Green's function is expressed as

$$G_{\text{loc}}^\sigma(i\omega_n) = \int \frac{\rho(\epsilon) d\epsilon}{i\omega_n + \mu - \epsilon - \Sigma_{\text{loc}}^\sigma(i\omega_n)}, \quad (4)$$

where $\rho(\epsilon)$ denotes the noninteracting density of states (DOS). For the hypercubic lattice, the noninteracting DOS is given by

$$\rho(\epsilon) = \frac{1}{\sqrt{\pi}D} \exp\left[-\left(\frac{\epsilon}{D}\right)^2\right], \quad (5)$$

where D is the characteristic energy. In the effective impurity model, the Weiss function is described by

$$\mathcal{G}^\sigma(i\omega_n)^{-1} = i\omega_n + \mu - \Delta^\sigma(i\omega_n), \quad (6)$$

where $\Delta^\sigma(i\omega_n)$ denotes the hybridization function [56]. The self-consistent equations in the framework of DMFT are given by $G_{\text{imp}}^\sigma(i\omega_n) = G_{\text{loc}}^\sigma(i\omega_n)$ and $\Sigma_{\text{imp}}^\sigma(i\omega_n) = \Sigma_{\text{loc}}^\sigma(i\omega_n)$. For given Weiss function, we solve the effective impurity model to compute the impurity Green's function $G_{\text{imp}}^\sigma(i\omega_n)$ and self-energy $\Sigma_{\text{imp}}^\sigma(i\omega_n)$, obtain the lattice Green's function $G_{\text{loc}}(i\omega_n)$, update the Weiss function, and iterate this self-consistent procedure until the result converges within numerical accuracy.

In this study, we employ the hybridization-expansion CTQMC method [78] as the impurity solver to systematically investigate low-temperature properties. Since we focus on the region $U \gg D$ and $T \ll D$, we adopt two established improvements to enhance efficiency and accuracy. First, the double-flip update [79] is employed to maintain a reasonable acceptance ratio in the strong-coupling regime. Second, we use the nonuniform sampling scheme [45] together with the intermediate representation basis [80, 81], which allows for an accurate representation of the Green's function. These improvements are essential for quantitatively analyzing the ferromagnetic instability at low temperatures in the strong-coupling regime.

In this calculation, we evaluate several physical quantities. The magnetic susceptibility is defined as

$$\chi_\alpha = \lim_{h \rightarrow 0} \frac{m_\alpha}{h_\alpha}, \quad (7)$$

where h_α is an external field that couples to the system via the Zeeman Hamiltonian $-h_\alpha \hat{S}_\alpha$. We note that the magnetic susceptibility is independent of α (see Appendix A for details) and therefore we evaluate it using a generator $\Lambda_N = \text{Diag}(\mathbf{v}_N)$ with $\mathbf{v}_N = \sqrt{2/[N(N-1)]}(1, 1, \dots, -(N-1))$ for simplicity. In this case, the magnetization is given by $m = \sqrt{(N-1)/(2N)}(n_1 - n_N)$. To discuss the stability of the FM state, we also evaluate the kinetic energy per site defined by $K = \sum_\sigma K_\sigma$ with $K_\sigma = -\int_0^\beta d\tau G_{\text{imp}}^\sigma(\tau) \Delta^\sigma(-\tau)$ and the interaction energy $I = U \sum d_{\sigma,\sigma'}/2$, where $d_{\sigma,\sigma'} [= \sum_i \langle \hat{n}_{i,\sigma} \hat{n}_{i,\sigma'} \rangle / L]$ is the double occupancy between flavors σ and σ' . In addition, we consider the following quantity

$$A_\sigma = -\frac{1}{\pi T} G_{\text{imp}}^\sigma\left(\frac{1}{2T}\right), \quad (8)$$

which, at zero temperature, reduces to the DOS at the Fermi level [82–85]. Thus, even at finite temperatures, A_σ allows us to discuss whether each flavor exhibits metallic or insulating behavior. In the following, examining several physical quantities, we discuss the ferromagnetic instability in the $SU(N)$ Fermi-Hubbard model.

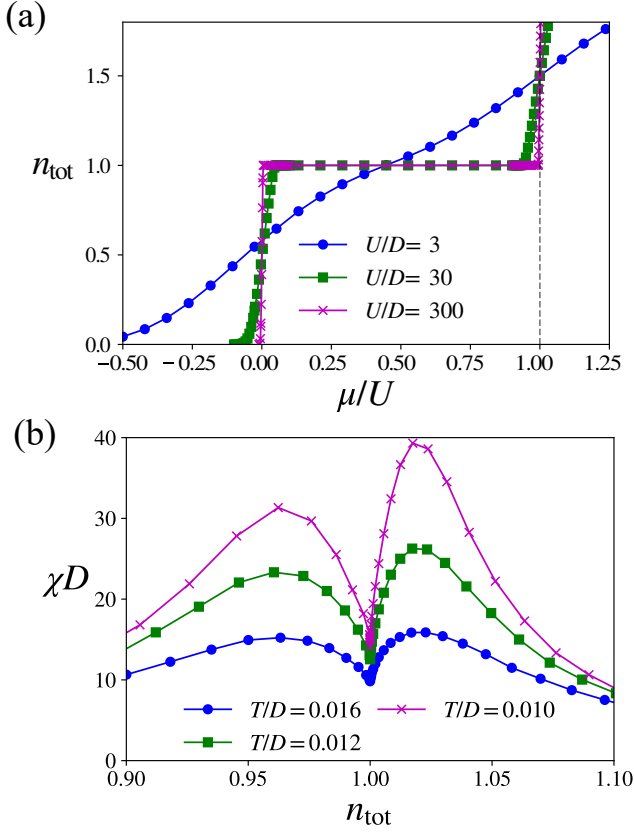


FIG. 1. (a) Total number of particles n_{tot} as a function of the chemical potential for the SU(3) Fermi-Hubbard model at $T/D = 0.01$ when $U/D = 3$ (blue), 30 (green), and 300 (magenta). The dashed line indicates the chemical potential corresponding to the half-filled condition. (b) Magnetic susceptibility as a function of n_{tot} for $U/D = 300$ when $T/D = 0.010$ (blue), 0.012 (green), and 0.016 (magenta).

III. NUMERICAL RESULTS

A. Ferromagnetism in the SU(3) Fermi-Hubbard model

We consider the SU(3) Fermi-Hubbard model to discuss its ferromagnetic instability. First, we examine the chemical potential dependence of the total number of particles. The results for $T/D = 0.01$ are shown in Fig. 1(a). We find that, as the chemical potential increases, n_{tot} smoothly increases in the weak-coupling case ($U/D = 3$), while a plateau appears at $n_{\text{tot}} = 1$ in the strong-coupling cases ($U/D = 30$ and 300). This plateau signals the formation of a Mott insulating phase at one-third filling [86]. In contrast, for the intermediate filling case with $n_{\text{tot}} \neq 1$, the filling varies smoothly with increasing μ , implying that metallic states are realized away from the commensurate filling.

To study the ferromagnetic instability in the system, we examine the magnetic susceptibility since its temperature dependence is useful for indicating the precursors of ferromagnetism [44, 45]. In Fig. 1(b), we show the magnetic sus-

ceptibility for $U/D = 300$ when $T/D = 0.010, 0.012$, and 0.016. We find two peaks below and above the one-third filling $n_{\text{tot}} = 1$. A notable feature is that the magnetic susceptibility around these peaks is significantly enhanced as the temperature decreases. The lower-density peak ($n_{\text{tot}} \sim 0.96$) reflects the well-established precursor of the generalized Nagaoka ferromagnetism, which has been investigated in detail in Ref. [45]. In addition to this, similar behavior appears in the higher-density regime ($n_{\text{tot}} \sim 1.02$), suggesting the formation of the FM state at low temperatures. In contrast, in the dilute limit ($n_{\text{tot}} \sim 0$), we find no peak singularity (not shown). This means that the ground state should be paramagnetic since particle correlations have little effect on the system.

To clarify whether the FM state is indeed realized around $n_{\text{tot}} \sim 1.02$, we calculate the temperature dependence of the particle density for each flavor for $U/D = 300$, as shown in Fig. 2(a). At higher temperatures, the paramagnetic (PM) state is realized with equal particle densities $n_1 = n_2 = n_3$. In contrast, we find a clear density imbalance at low temperatures, which indicates spontaneous symmetry breaking. Since $n_1 = n_2 \neq n_3$, the FM state is characterized by v_3 . As the temperature increases, the imbalance in particle density decreases and suddenly vanishes at $T = T_{c_2} (\sim 0.0066D)$. This implies that the first-order magnetic phase transition occurs to the PM state, which is essentially the same as the ferromagnetic transition in the hole-doped case [45]. The solution survives down to $T = T_{c_1} (\sim 0.0055D)$.

One of the most important points is that $n_1 = n_2$ approaches 0.5 with decreasing temperature, which suggests that a Mott insulating state is realized for flavors $\sigma = 1$ and 2. To confirm this, we examine the double occupancy $d_{\sigma,\sigma'}$ and the quantity A_σ , as shown in Figs. 2(b) and 2(c). The latter may be regarded as the DOS at Fermi level. As the temperature decreases, we find $d_{12} \ll d_{23} = d_{31}$. Furthermore, we find that A_σ for flavors $\sigma = 1, 2$ approach zero, whereas the other remains finite. These results indicate that flavors $\sigma = 1, 2$ become Mott insulating, while flavor $\sigma = 3$ remains metallic. This demonstrates that the ferromagnetic order is accompanied by a spontaneous flavor-selective Mott state [29, 87–89]. This naturally suggests that, in the zero temperature limit, one particle occupies either flavor 1 or 2 at each site, while remaining particles freely move in the other flavor. To further clarify this, the noninteracting DOS at the Fermi level for the particle density $n_3 = 0.02$ is shown as a red dashed line in Fig. 2(b). We find that A_3 asymptotically approaches this value with decreasing temperatures, providing additional evidence that, in the FM phase, particles with flavor $\sigma = 3$ are effectively non-interacting whereas particles with the other flavors are completely localized. This conclusion is further supported by analyzing the energy gain, whose dominant contribution arises from the kinetic energy of flavor $\sigma = 3$ (not shown).

We also discuss the stability of the FM state against the interaction strength. The magnetization m and the inverse susceptibility $1/(\chi D)$ for $T/D = 0.003$ and $n_{\text{tot}} = 1.02$ are shown in Fig. 3. When U is small, the PM state is realized with $n_\sigma = n_{\text{tot}}/3$ and $m = 0$. The susceptibility increases with increasing interaction strength. The PM solution suddenly vanishes at $U = U_{c_1}$ ($U_{c_1}/D \sim 90$), and spontaneous magneti-

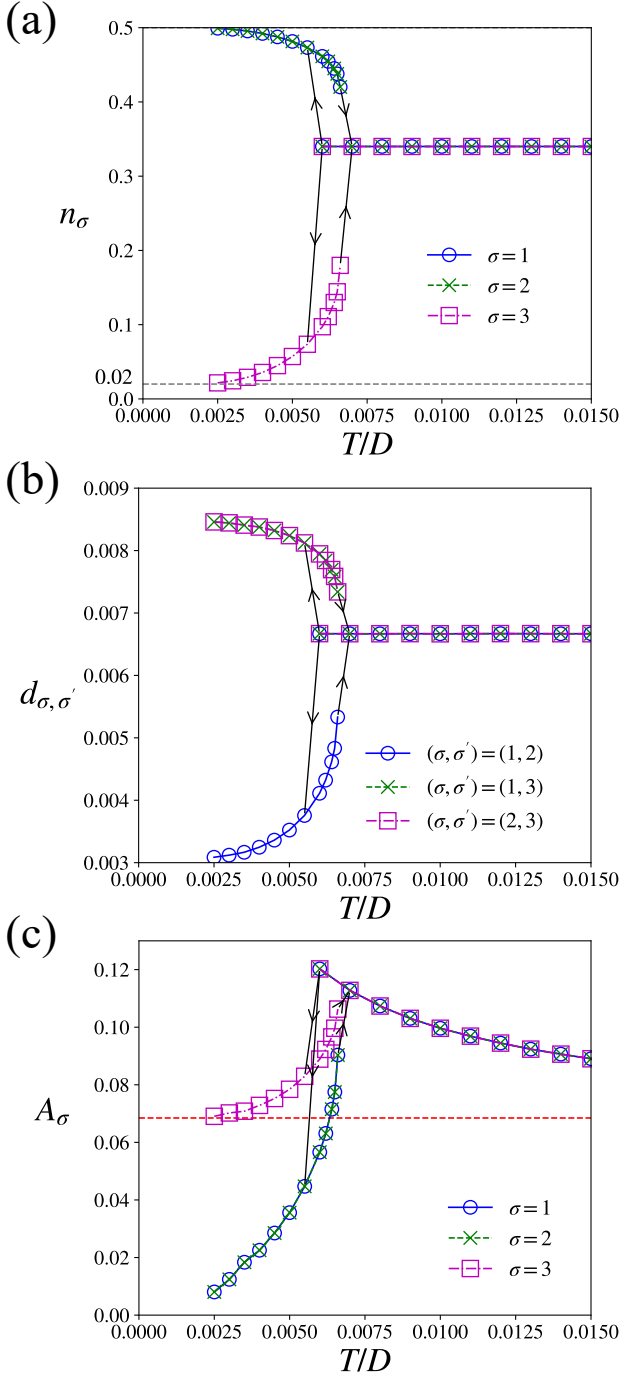


FIG. 2. (a) Particle density n_σ , (b) double occupancy $d_{\sigma,\sigma'}$, and (c) the quantity A_σ in the SU(3) Fermi-Hubbard model with $U/D = 300$ and $n_{\text{tot}} = 1.02$. The red dashed line in (c) represents the value of the noninteracting DOS corresponding to $n_3 = 0.02$.

zation emerges. A further increase in the interaction strength leads to a monotonic increase in the magnetization. This behavior contrasts with that of the antiferromagnetically ordered state stabilized by the Heisenberg interaction $J \sim D^2/U$, where the magnetization is suppressed in the strong-coupling

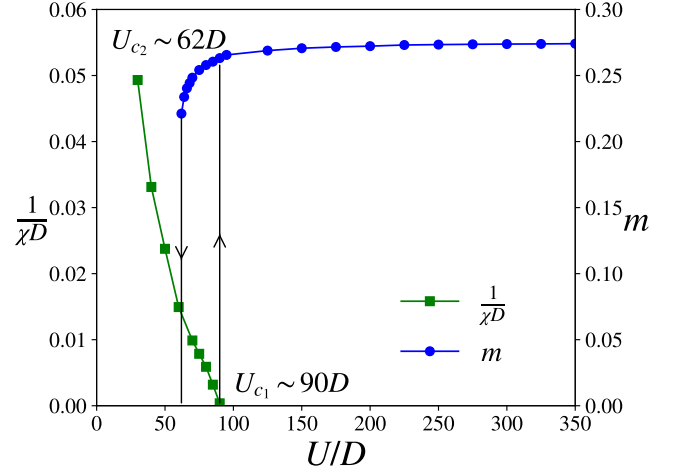


FIG. 3. Magnetization m (right axis) and inverse magnetic susceptibility $1/\chi D$ (left axis) as functions of the interaction strength U/D for the SU(3) Fermi-Hubbard model at $T/D = 0.003$ and $n_{\text{tot}} = 1.02$.

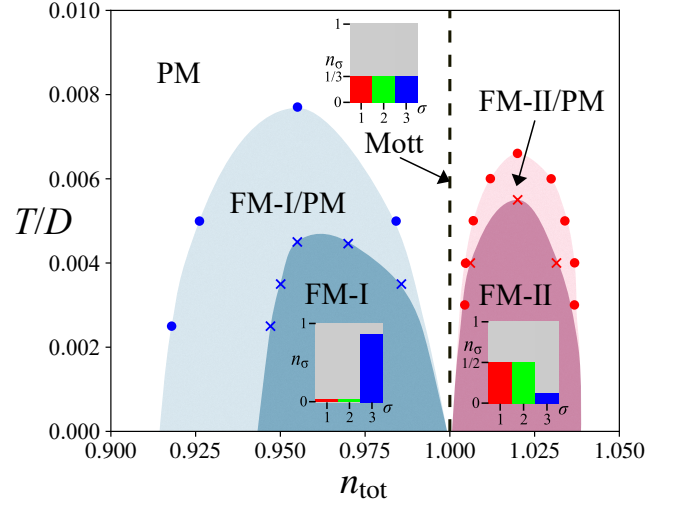


FIG. 4. Finite-temperature phase diagram of the SU(3) Fermi-Hubbard model for $U/D = 300$ around one-third filling ($n_{\text{tot}} \sim 1$). Blue (red) circles and crosses represent the phase transition points, where FM-I (FM-II) and PM states disappear, respectively. The Mott insulating state at one-third filling $n_{\text{tot}} = 1$ is indicated by the dashed line. The flavor occupancies for FM-I, FM-II, and Mott states are illustrated.

regime at finite temperatures. When the interaction strength decreases from the strong-coupling regime, the magnetization abruptly vanishes at $U = U_{c_2}$ ($U_{c_2}/D \sim 62$). Therefore, the system undergoes a first-order magnetic phase transition accompanied by hysteresis. In the region $U_{c_2} < U < U_{c_1}$, both FM and PM solutions coexist.

We show in Fig. 4 the phase diagram of the SU(3) Fermi-Hubbard model on the hypercubic lattice. We find that two FM phases (FM-I and FM-II) are realized both below and

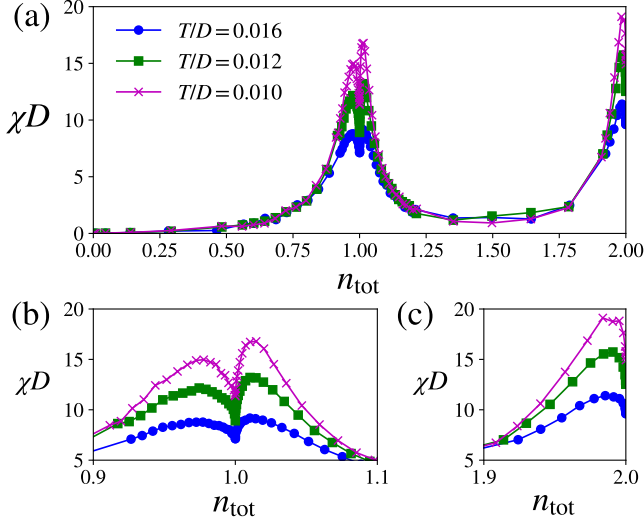


FIG. 5. (a) Overall behavior of the susceptibility as a function of n_{tot} in the SU(4) Fermi-Hubbard model for $U/D = 300$ when $T/D = 0.01, 0.012$, and 0.016 . (b) [(c)] Enlarged views of the regions around $n_{\text{tot}} = 1$ ($n_{\text{tot}} = 2$).

above one-third filling ($n_{\text{tot}} = 1$). The FM-I phase is characterized by Nagaoka ferromagnetism, where two of three flavors are empty and the other is metallic. By contrast, in the FM-II state, two of three flavors are Mott insulating and the other is metallic. Therefore, both FM-I and FM-II phases are characterized by v_3 , with negative and positive values, respectively. At the commensurate filling $n_{\text{tot}} = 1$, the Mott insulating state is stabilized up to a fairly large temperature, which is proportional to the interaction strength U . These results indicate that, even in the strong-coupling limit ($U \rightarrow \infty$), the Mott insulating state with $m = 0$ appears at the commensurate filling, implying that FM-I and FM-II states cannot be continuously connected. This should be consistent with the fact that the filling occupations for the dominant flavors differ among these states, as illustrated in Fig. 4.

We wish to comment on the effect of the lattice geometry on the stability of the FM states. It has been clarified that the FM-I state appears on the hypercubic lattice, while is not stabilized on the Bethe lattice. Similar behavior is also observed in the case with $n_{\text{tot}} > 1$. In fact, no peak structure appears in the susceptibility near $n_{\text{tot}} \sim 1.02$ (see Appendix B) and we could not find the FM state at low temperatures. This suggests that, even in the FM-II case, the presence of closed-loops in the lattice plays an essential role in stabilizing the FM states.

B. Ferromagnetism in the SU(4) Fermi-Hubbard model

We also consider the ferromagnetic instability of the SU(4) Fermi-Hubbard model on the hypercubic lattice. Figure 5 shows the filling dependence of the magnetic susceptibility for $U/D = 300$ when $T/D = 0.01, 0.012$, and 0.016 . We find that magnetic fluctuations develop around $n \sim 0.97, 1.01$ and

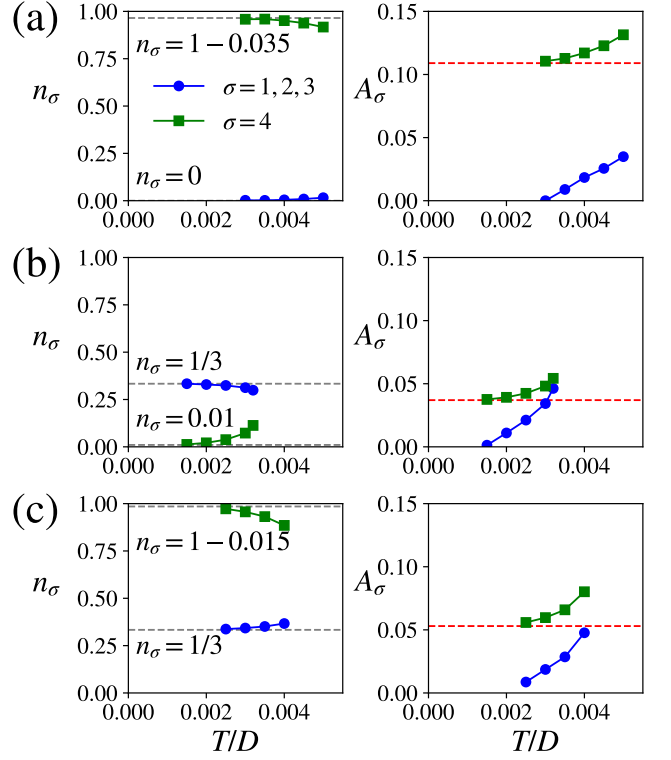


FIG. 6. Temperature dependence of the particle density n_σ (left panels) and the quantity A_σ (right panels) in the SU(4) Fermi-Hubbard model for $U/D = 300$ when (a) $n_{\text{tot}} = 0.965$, (b) $n_{\text{tot}} = 1.01$, and (c) $n_{\text{tot}} = 1.985$, respectively. Blue circles (green squares) represent the results for the flavors $\sigma = 1, 2, 3$ ($\sigma = 4$). The red dashed lines in left panel of (a), (b), and (c) indicate the value of the noninteracting DOS corresponding to $n_4 = 0.965, 0.01$, and 0.985 , respectively.

1.99 with decreasing temperature, indicating that the FM state is likely to appear even in the SU(4) model.

Figure 6 shows the temperature dependence of the particle density n_σ for (a) $n_{\text{tot}} = 0.965$, (b) $n_{\text{tot}} = 1.01$, and (c) $n_{\text{tot}} = 1.985$. We find a clear particle-density imbalance at low temperatures, implying that the FM states are indeed stabilized at low temperatures. For the hole-doped region away from quarter filling ($n_{\text{tot}} = 0.965$), the system realizes a FM phase dominated by a single flavor (FM-I), whereas on the particle-doped side ($n_{\text{tot}} = 1.01$), a distinct FM state emerges in which three flavors acquire large occupations (FM-II). In addition, below half filling ($n_{\text{tot}} = 1.985$), another FM state (FM-III) appears, characterized by the dominant contribution of one flavor while the other three flavors remain partially populated. We further observe that the four flavors separate into two groups: three flavors satisfy $n_\sigma = 0$ or $1/3$, while the remaining flavor has an intermediate occupation. This indicates that the FM-I (FM-II and FM-III) state consists of band (Mott) insulating behavior in the major flavors, while the minor flavor stays metallic. This is consistent with the fact that $A_1 = A_2 = A_3 \sim 0$ and $A_4 \neq 0$ at low temperatures, as shown in Fig. 6. Therefore, these states with spontaneous symme-

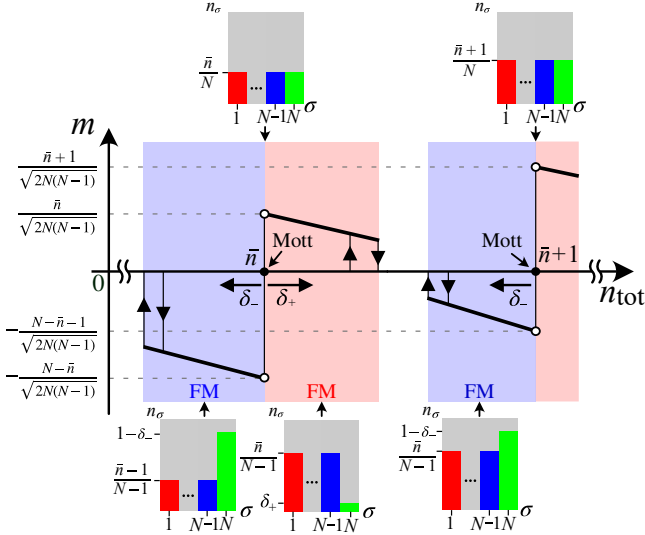


FIG. 7. Schematic illustration of the FM states near the commensurate fillings. The horizontal axis represents the total particle density n_{tot} , and the vertical axis indicates the magnetization m .

try breaking are characterized by v_4 . Given the considerable computational cost of the systematic analysis, obtaining a quantitative finite-temperature phase diagram is challenging. However, our results demonstrate that, owing to particle-hole symmetry of the system, six types of the FM states emerge near the commensurate fillings $n_{\text{tot}} = 1, 2$, and 3.

C. Ferromagnetism in the $SU(N)$ Fermi-Hubbard model

We now discuss the nature of the FM ground-state in the $SU(N)$ Fermi-Hubbard model. It has been clarified that, near the commensurate fillings ($n_{\text{tot}} = 1, 2, \dots, N-1$), magnetic fluctuations are strongly enhanced and the FM state is stabilized at low temperatures under strong interactions. When the holes are doped in the system with $1/N$ filling ($n_{\text{tot}} = 1$), the FM state consists of $N-1$ empty flavors and one metallic flavor. This state is naturally interpreted as a generalization of Nagaoka ferromagnetism. By contrast, in the other FM states found in our analysis, the Mott insulating state is realized in $N-1$ flavors and the other remains metallic. Therefore, these ordered states can be characterized by the spontaneous flavor-selective Mott state with the flavor imbalance vector v_N . A key point is that $(N-1)$ flavors are band or Mott insulating while the remaining flavor stays itinerant due to the lack of interaction-energy cost for hopping. Since the kinetic energy of this itinerant flavor stabilizes the ordered state, they may be regarded as the generalized Nagaoka ferromagnetism extended to the commensurate fillings.

Figure 7 schematically illustrates the flavor occupations of the FM states in the $SU(N)$ Fermi-Hubbard model with $T = 0$ and $U \rightarrow \infty$. Consider the system around a certain commensurate filling $n_{\text{tot}} = \bar{n}$ with integer $\bar{n} (= 1, 2, \dots, N-1)$. It is well known that, at the commensurate filling ($n_{\text{tot}} = \bar{n}$), the

Mott insulating state is realized, where the particle density for each flavor is fractional ($n_\sigma = \bar{n}/N$). When $n_{\text{tot}} = \bar{n} - \delta_-$ with a small positive value δ_- , the FM state is expected to appear. In this case, the particle density of flavors $\sigma = 1, \dots, N-1$ is $(\bar{n}-1)/(N-1)$, while that of flavor $\sigma = N$ is $1 - \delta_-$, leading to a negative magnetization. On the other hand, when $n_{\text{tot}} = \bar{n} + \delta_+$ with a small positive value δ_+ , the particle density of flavors $\sigma = 1, \dots, N-1$ is $\bar{n}/(N-1)$, while that of flavor $\sigma = N$ is δ_+ . In this case, the magnetization becomes positive. Since the Mott insulating state is realized at the commensurate filling, the above two FM states cannot be adiabatically connected to each other. On the other hand, it may be non-trivial whether two FM states with the same configuration in the $(N-1)$ flavors, which are located at $n_{\text{tot}} = \bar{n} + \delta_+$ and $n_{\text{tot}} = (\bar{n} + 1) - \delta_-$, are adiabatically connected. Since the particle density in the remaining flavor is either nearly empty or nearly fully occupied, a sign change in the magnetization naturally occurs. Furthermore, we have observed that the FM states in the $SU(2)$ [44], $SU(3)$, and $SU(4)$ cases are not stable for large δ_- and δ_+ . Therefore, we expect that a total of $2(N-1)$ distinct FM states emerge in the $SU(N)$ Fermi-Hubbard model.

IV. CONCLUSIONS

We have investigated the $SU(N)$ Fermi-Hubbard model on the hypercubic lattice, employing DMFT combined with the CTQMC method. In the $SU(3)$ Fermi-Hubbard model above one-third filling, we have found that the FM state appears at low temperatures under strong interactions, accompanied by a spontaneous flavor-selective Mott state where two flavors are Mott insulating and the remaining flavor is metallic. Extending the analysis to $SU(4)$, we have identified six distinct types of FM states away from the commensurate fillings. We have also discussed the ferromagnetic instability of the $SU(N)$ Fermi-Hubbard model. Overall, our results clarify the origin of ferromagnetism in $SU(N)$ Fermi-Hubbard systems and reveal their rich magnetic behavior. Since $SU(N)$ -symmetric systems have been realized with ultracold atomic gases [15–20, 23, 24], our results can be tested experimentally, e.g., by using quantum gas microscopes [90, 91].

In our study, we have restricted our analysis to magnetic orders characterized by a spatially uniform order parameter since we have focused on strong particle correlations in the $SU(N)$ Fermi-Hubbard model away from commensurate fillings as a first step. Clarifying how ordered states with enlarged unit cells—such as antiferromagnetic [92–94] and canted magnetic orders [95–98]—compete with the FM state remains an important direction for future work and will be addressed elsewhere.

ACKNOWLEDGMENTS

This work was supported by JSPS KAKENHI Grants No. JP22K03525, JP25H01521, JP25H01398 (A.K.), No. JP25K17327 (K.Y.). This work was partly funded by Hirose

Foundation, the Precise Measurement Technology Promotion Foundation, and the Fujikura Foundation. Parts of the numerical calculations were performed in the supercomputing systems in ISSP, the University of Tokyo. Parts of the simulations have been performed using the ALPS libraries [99].

Appendix A: Isotropy of the magnetic susceptibility

Here, we clarify that the magnetic susceptibility is isotropic in the PM state. For convenience, we present the diagonal generators of $SU(N)$ in the following explicit form:

$$\lambda_\alpha = \sqrt{\frac{2}{\alpha(\alpha+1)}} I_\alpha \oplus (-\alpha)I_1 \oplus \tilde{0}_{N-\alpha-1} \quad (\alpha = 1, \dots, N-1), \quad (A1)$$

where I_k and $\tilde{0}_k$ denote the k -dimensional identity and zero matrix, respectively. This definition satisfies the orthonormality condition $\text{Tr}(\lambda_\alpha \lambda_\beta) = 2\delta_{\alpha\beta}$.

Then, the external field term for an arbitrary direction can be written as

$$\hat{H}_{\text{ext}} = - \sum_{\alpha=1}^{N-1} h_\alpha \hat{S}_\alpha. \quad (A2)$$

Here, the external field used in the main part of the paper corresponds to choosing $h_{N-1} \neq 0$ and $h_\alpha = 0$ for $\alpha = 1, \dots, N-2$. The corresponding change in the chemical potential per flavor induced by the external field is given by

$$(\Delta\mu)_\sigma = - \sum_{\alpha=1}^{N-1} \frac{h_\alpha}{2} (\lambda_\alpha)_{\sigma,\sigma}. \quad (A3)$$

When the interaction strength and temperature are fixed, the vector $\mathbf{n} \equiv (n_1, \dots, n_N)$ depends only on the chemical potential. Accordingly, it can be expanded as

$$\mathbf{n}(\mu + \Delta\mu) = \mathbf{n}(\mu) + \mathbf{J}_n(\mu) \Delta\mu + O(|\Delta\mu|^2), \quad (A4)$$

where $[\mathbf{J}_n(\mu)]_{i,j} \equiv \partial n_i / \partial \mu_j$, and the exchange symmetry among flavors ensures that the diagonal and off-diagonal components of the Jacobian matrix $\mathbf{J}_n(\mu)$ take the same value as $d \equiv [\mathbf{J}_n(\mu)]_{i,i}$ and $o \equiv [\mathbf{J}_n(\mu)]_{i \neq j}$, respectively.

The magnitude of total magnetization can be expressed in terms of the particle densities as

$$\tilde{m} \equiv \sqrt{\sum_{\alpha=1}^{N-1} m_\alpha^2} = \sqrt{\frac{1}{2} \left(\sum_{\sigma} n_\sigma^2 \right) - \frac{1}{2N} \left(\sum_{\sigma} n_\sigma \right)^2}. \quad (A5)$$

When the external field is sufficiently weak, using Eq. (A4),

we obtain

$$\tilde{m}^2 \simeq \frac{(o-d)^2}{2} \sum_{\sigma} (\Delta\mu)_\sigma^2 + \frac{1}{2} \{2od + (N-2)o^2\} \left(\sum_{\sigma} (\Delta\mu)_\sigma \right)^2. \quad (A6)$$

From the orthonormality relation of the generalized Gell-Mann matrices, the first term satisfies $\sum_{\sigma} (\Delta\mu)_\sigma^2 = h^2/2$, where $h \equiv \sqrt{\sum_a |h_a|^2}$ denotes the magnitude of the external field. The second term vanishes because the trace of the matrices is zero. Therefore, the magnetic susceptibility is given by

$$\chi = \lim_{h \rightarrow 0} \frac{\tilde{m}}{h} = \frac{|o-d|}{2}, \quad (A7)$$

which is independent of the direction of the external field, demonstrating the isotropy of the magnetic susceptibility.

Appendix B: Magnetic susceptibility on the Bethe lattice

Here, we investigate magnetic fluctuations in the $SU(3)$ Fermi-Hubbard model above one-third filling on the Bethe lattice, which has the infinite coordination number and also provides an exact solution within DMFT framework. In the Bethe lattice, the number of nearest neighbor sites is the same for all sites, and it does not contain closed loops. This implies that the generalized Nagaoka's theorem that ensures the existence of the FM state is not applicable [40, 50]. Indeed, it has been suggested that below one-third filling, the ferromagnetic order does not appear on the Bethe lattice [45].

The noninteracting DOS is given by

$$\rho(\epsilon) = \frac{2}{\pi D} \sqrt{1 - \left(\frac{\epsilon}{D}\right)^2}, \quad (B1)$$

which leads to the simple Dyson equation for the effective impurity model as

$$\mathcal{G}^\sigma(i\omega_n)^{-1} = i\omega_n + \mu - \frac{D^2}{4} G_{\text{loc}}^\sigma(i\omega_n). \quad (B2)$$

Combining Eq. (B2) with Eq. (6) yields the self-consistent equation in the imaginary-time domain as $\Delta^\sigma(\tau) = \frac{D^2}{4} G_{\text{loc}}^\sigma(\tau)$.

Figure 8 shows the filling dependence of the magnetic susceptibility for the $SU(3)$ -symmetric case on the Bethe lattice above one-third filling. In contrast to the hypercubic lattice, where the susceptibility shows a peak structure above one-third filling (see Fig. 1), such nonmonotonic behavior is not observed on the Bethe lattice for any temperatures. Since the emergence of a ferromagnetic order is accompanied by an enhancement of magnetic fluctuations, this result suggests that the FM state does not appear above one-third filling on the Bethe lattice, which is similar to the $SU(2)$ - and $SU(3)$ -symmetric cases [44, 45]. These results indicate that the emergence of ferromagnetism near commensurate fillings in the $SU(N)$ Fermi-Hubbard model fairly depends on the lattice geometry.

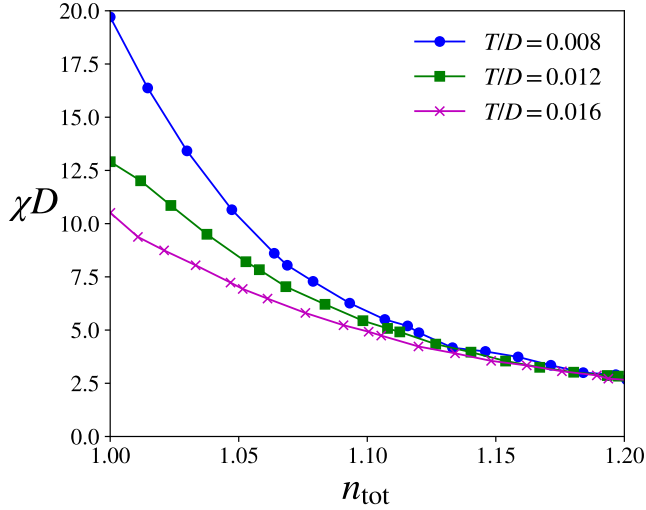


FIG. 8. Filling dependence of the susceptibility χD in the SU(3)-symmetric case on a Bethe lattice for $U/D = 300$. Blue, green, and magenta lines correspond to $T/D = 0.008, 0.012$, and 0.016 , respectively.

-
- [1] F. Schäfer, T. Fukuhara, S. Sugawa, Y. Takasu, and Y. Takahashi, Tools for quantum simulation with ultracold atoms in optical lattices, *Nat. Rev. Phys.* **2**, 411 (2020).
- [2] D. Greif, T. Uehlinger, G. Jotzu, L. Tarruell, and T. Esslinger, Short-range quantum magnetism of ultracold fermions in an optical lattice, *Science* **340**, 1307 (2013).
- [3] R. A. Hart, P. M. Duarte, T.-L. Yang, X. Liu, T. Paiva, E. Khatami, R. T. Scalettar, N. Trivedi, D. A. Huse, and R. G. Hulet, Observation of antiferromagnetic correlations in the Hubbard model with ultracold atoms, *Nature* **519**, 211 (2015).
- [4] M. Boll, T. A. Hilker, G. Salomon, A. Omran, J. Nespolo, L. Pollet, I. Bloch, and C. Gross, Spin-and density-resolved microscopy of antiferromagnetic correlations in Fermi-Hubbard chains, *Science* **353**, 1257 (2016).
- [5] M. F. Parsons, A. Mazurenko, C. S. Chiu, G. Ji, D. Greif, and M. Greiner, Site-resolved measurement of the spin-correlation function in the Fermi-Hubbard model, *Science* **353**, 1253 (2016).
- [6] L. W. Cheuk, M. A. Nichols, K. R. Lawrence, M. Okan, H. Zhang, E. Khatami, N. Trivedi, T. Paiva, M. Rigol, and M. W. Zwierlein, Observation of spatial charge and spin correlations in the 2D Fermi-Hubbard model, *Science* **353**, 1260 (2016).
- [7] C. He, E. Hajiyevev, Z. Ren, B. Song, and G.-B. Jo, Recent progresses of ultracold two-electron atoms, *J. Phys. B: Atomic, Molecular and Optical Physics* **52**, 102001 (2019).
- [8] M. Lebrat, M. Xu, L. H. Kendrick, A. Kale, Y. Gang, P. Seetharaman, I. Morera, E. Khatami, E. Demler, and M. Greiner, Observation of Nagaoka polarons in a Fermi-Hubbard quantum simulator, *Nature* **629**, 317 (2024).
- [9] C. Chin, R. Grimm, P. Julienne, and E. Tiesinga, Feshbach resonances in ultracold gases, *Rev. Mod. Phys.* **82**, 1225 (2010).
- [10] R. Grimm, M. Weidemüller, and Y. B. Ovchinnikov, Optical dipole traps for neutral atoms, *Adv. At. Mol. Opt. Phys.* **42**, 95 (2000).
- [11] B. DeMarco and D. S. Jin, Onset of fermi degeneracy in a trapped atomic gas, *Science* **285**, 1703 (1999).
- [12] A. G. Truscott, K. E. Strecker, W. I. McAlexander, G. B. Partridge, and R. G. Hulet, Observation of fermi pressure in a gas of trapped atoms, *Science* **291**, 2570 (2001).
- [13] F. Schreck, L. Khaykovich, K. L. Corwin, G. Ferrari, T. Bourdel, J. Cubizolles, and C. Salomon, Quasipure bose-einstein condensate immersed in a fermi sea, *Physical Review Letters* **87**, 080403 (2001).
- [14] S. R. Granade, M. E. Gehm, K. M. O'Hara, and J. E. Thomas, All-optical production of a degenerate fermi gas, *Physical Review Letters* **88**, 120405 (2002).
- [15] T. Fukuhara, Y. Takasu, M. Kumakura, and Y. Takahashi, Degenerate fermi gases of ytterbium, *Phys. Rev. Lett.* **98**, 030401 (2007).
- [16] S. Taie, Y. Takasu, S. Sugawa, R. Yamazaki, T. Tsujimoto, R. Murakami, and Y. Takahashi, Realization of a SU(2) × SU(6) system of fermions in a cold atomic gas, *Phys. Rev. Lett.* **105**, 190401 (2010).
- [17] Pasqualetti, G. and Bettermann, O. and Darkwah Oppong, N. and Ibarra-García-Padilla, E. and Dasgupta, S. and Scalettar, R. T. and Hazzard, K. R. A. and Bloch, I. and Fölling, S., Equation of State and Thermometry of the 2D SU(N) Fermi-Hubbard Model, *Phys. Rev. Lett.* **132**, 083401 (2024).
- [18] G. Pagano, M. Mancini, G. Cappellini, P. Lombardi, F. Schäfer, H. Hu, X.-J. Liu, J. Catani, C. Sias, M. Inguscio, *et al.*, A one-dimensional liquid of fermions with tunable spin, *Nat Phys* **10**, 198 (2014).
- [19] B. J. DeSalvo, M. Yan, P. G. Mickelson, Y. N. Martinez de Escobar, and T. C. Killian, Degenerate fermi gas of ^{87}Sr , *Phys. Rev. Lett.* **105**, 030402 (2010).
- [20] X. Zhang, M. Bishof, S. L. Bromley, C. V. Kraus, M. S. Safronova, P. Zoller, A. M. Rey, and J. Ye, Spectroscopic obser-

- vation of $su(n)$ -symmetric interactions in sr orbital magnetism, *science* **345**, 1467 (2014).
- [21] J. Hubbard, Electron correlations in narrow energy bands, *Proc. R. Soc. Lond. A* **276**, 238 (1963).
- [22] C. Honerkamp and W. Hofstetter, Ultracold fermions and the $SU(n)$ hubbard model, *Phys. Rev. Lett.* **92**, 170403 (2004).
- [23] C. Hofrichter, L. Riegger, F. Scazza, M. Höfer, D. R. Fernandes, I. Bloch, and S. Fölling, Direct Probing of the Mott Crossover in the $SU(N)$ Fermi-Hubbard Model, *Phys. Rev. X* **6**, 021030 (2016).
- [24] H. Ozawa, S. Taie, Y. Takasu, and Y. Takahashi, Antiferromagnetic Spin Correlation of $SU(N)$ Fermi Gas in an Optical Superlattice, *Phys. Rev. Lett.* **121**, 225303 (2018).
- [25] S. Taie, E. Ibarra-García-Padilla, N. Nishizawa, Y. Takasu, Y. Kuno, H.-T. Wei, R. T. Scalettar, K. R. Hazzard, and Y. Takahashi, Observation of antiferromagnetic correlations in an ultracold $SU(N)$ Hubbard model, *Nat. Phys.* **18**, 1356 (2022).
- [26] C. Wu, J.-p. Hu, and S.-c. Zhang, Exact $SO(5)$ Symmetry in the Spin-3/2 Fermionic System, *Phys. Rev. Lett.* **91**, 186402 (2003).
- [27] C. Honerkamp and W. Hofstetter, Ultracold Fermions and the $SU(N)$ Hubbard Model, *Phys. Rev. Lett.* **92**, 170403 (2004).
- [28] M. Hermele, V. Gurarie, and A. M. Rey, Mott Insulators of Ultracold Fermionic Alkaline Earth Atoms: Underconstrained Magnetism and Chiral Spin Liquid, *Phys. Rev. Lett.* **103**, 135301 (2009).
- [29] A. Rapp and A. Rosch, Ground-state phase diagram of the repulsive $SU(3)$ Hubbard model in the Gutzwiller approximation, *Phys. Rev. A* **83**, 053605 (2011).
- [30] M. A. Cazalilla and A. M. Rey, Ultracold Fermi gases with emergent $SU(N)$ symmetry, *Rep. Prog. Phys.* **77**, 124401 (2014).
- [31] S. Capponi, P. Lecheminant, and K. Totsuka, Phases of one-dimensional $SU(N)$ cold atomic Fermi gases—From molecular Luttinger liquids to topological phases, *Annu. Pyhs.* **367**, 50 (2016).
- [32] H. Yoshida and H. Katsura, Rigorous Results on the Ground State of the Attractive $SU(N)$ Hubbard Model, *Phys. Rev. Lett.* **126**, 100201 (2021).
- [33] K. Yamamoto and N. Kawakami, Universal description of dissipative Tomonaga-Luttinger liquids with $SU(N)$ spin symmetry: Exact spectrum and critical exponents, *Phys. Rev. B* **107**, 045110 (2023).
- [34] C. Feng, E. Ibarra-García-Padilla, K. R. A. Hazzard, R. Scalettar, S. Zhang, and E. Vitali, Metal-insulator transition and quantum magnetism in the $su(3)$ fermi-hubbard model, *Phys. Rev. Res.* **5**, 043267 (2023).
- [35] M. Nakagawa, H. Katsura, and M. Ueda, Exact eigenstates of multicomponent Hubbard models: $SU(N)$ magnetic η pairing, weak ergodicity breaking, and partial integrability, *Phys. Rev. Res.* **6**, 043259 (2024).
- [36] E. Ibarra-García-Padilla and S. Choudhury, Many-body physics of ultracold alkaline-earth atoms with $SU(N)$ -symmetric interactions, *J. Phys.: Condens. Matter* **37**, 083003 (2024).
- [37] J. C. Slater, The ferromagnetism of nickel, *Phys. Rev.* **49**, 537 (1936).
- [38] A. Mielke, Ferromagnetism in the hubbard model on line graphs and further considerations, *Journal of Physics A: Mathematical and General* **24**, 3311 (1991).
- [39] H. Tasaki, Ferromagnetism in the hubbard models with degenerate single-electron ground states, *Phys. Rev. Lett.* **69**, 1608 (1992).
- [40] Y. Nagaoka, Ferromagnetism in a Narrow, Almost Half-Filled s Band, *Phys. Rev.* **147**, 392 (1966).
- [41] T. Obermeier, T. Pruschke, and J. Keller, Ferromagnetism in the large- U Hubbard model, *Phys. Rev. B* **56**, R8479 (1997).
- [42] R. Zitzler, T. Pruschke, and R. Bulla, Magnetism and phase separation in the ground state of the Hubbard model, *Eur. Phys. J. B* **27**, 473 (2002).
- [43] H. Park, K. Haule, C. A. Marianetti, and G. Kotliar, Dynamical mean-field theory study of Nagaoka ferromagnetism, *Phys. Rev. B* **77**, 035107 (2008).
- [44] Y. Kamogawa, J. Nasu, and A. Koga, Ferromagnetic instability for the single-band Hubbard model in the strong-coupling regime, *Phys. Rev. B* **99**, 235107 (2019).
- [45] J. Fujii, K. Yamamoto, and A. Koga, Itinerant ferromagnetism in an $su(3)$ fermi-hubbard model at finite temperatures: A dynamical mean-field theory study, *Phys. Rev. B* **112**, 115136 (2025).
- [46] R. Samajdar and R. N. Bhatt, Polaronic mechanism of Nagaoka ferromagnetism in Hubbard models, *Phys. Rev. B* **109**, 235128 (2024).
- [47] C.-H. Huang and M. A. Cazalilla, Itinerant ferromagnetism in $SU(N)$ -symmetric fermi gases at finite temperature: first order phase transitions and time-reversal symmetry, *New J. Phys.* **25**, 063005 (2023).
- [48] P. Sharma, Y. Peng, D. N. Sheng, H. J. Changlani, and Y. Wang, Nagaoka instability and quantum phase transition via kinetic frustration control, *arXiv preprint arXiv:2508.08410* (2025).
- [49] M. A. Cazalilla, A. Ho, and M. Ueda, Ultracold gases of ytterbium: ferromagnetism and Mott states in an $SU(6)$ Fermi system, *New J. Phys.* **11**, 103033 (2009).
- [50] H. Katsura and A. Tanaka, Nagaoka states in the $SU(n)$ Hubbard model, *Phys. Rev. A* **87**, 013617 (2013).
- [51] R. R. P. Singh and J. Oitmaa, Divergence of magnetic susceptibility in the $SU(N)$ Nagaoka-Thouless ferromagnet, *Phys. Rev. B* **106**, 014424 (2022).
- [52] K.-S. Kim and V. Elser, Itinerant Ferromagnetism from One-Dimensional Mobility, *arXiv:2412.03638*.
- [53] A. Sotnikov and W. Hofstetter, Magnetic ordering of three-component ultracold fermionic mixtures in optical lattices, *Phys. Rev. A* **89**, 063601 (2014).
- [54] W. Metzner and D. Vollhardt, Correlated Lattice Fermions in $d = \infty$ Dimensions, *Phys. Rev. Lett.* **62**, 324 (1989).
- [55] E. Müller-Hartmann, Correlated fermions on a lattice in high dimensions, *Z. Phys. B* **74**, 507 (1989).
- [56] A. Georges, G. Kotliar, W. Krauth, and M. J. Rozenberg, Dynamical mean-field theory of strongly correlated fermion systems and the limit of infinite dimensions, *Rev. Mod. Phys.* **68**, 13 (1996).
- [57] G. Kotliar and H. Kajueter, Effects of orbital degeneracy on the mott transition in infinite dimensions, *Phys. Rev. B* **54**, R14221 (1996).
- [58] M. J. Rozenberg, Integer-filling metal-insulator transitions in the degenerate hubbard model, *Phys. Rev. B* **55**, R4855 (1997).
- [59] J. E. Han, M. Jarrell, and D. L. Cox, Multiorbital hubbard model in infinite dimensions: Quantum monte carlo calculation, *Phys. Rev. B* **58**, R4199 (1998).
- [60] A. Koga, Y. Imai, and N. Kawakami, Stability of a metallic state in the two-orbital hubbard model, *Phys. Rev. B* **66**, 165107 (2002).
- [61] Y. Ōno, M. Potthoff, and R. Bulla, Mott transitions in correlated electron systems with orbital degrees of freedom, *Phys. Rev. B* **67**, 035119 (2003).
- [62] A. Koga, N. Kawakami, T. M. Rice, and M. Sigrist, Orbital-selective mott transitions in the degenerate hubbard model, *Phys. Rev. Lett.* **92**, 216402 (2004).
- [63] A. Koga, N. Kawakami, T. M. Rice, and M. Sigrist, Spin,

- charge, and orbital fluctuations in a multi-orbital mott insulator, Phys. Rev. B **72**, 045128 (2005).
- [64] M. Capone, M. Fabrizio, and E. Tosatti, Direct transition between a singlet mott insulator and a superconductor, Phys. Rev. Lett. **86**, 5361 (2001).
- [65] Á. Rapp, G. Zaránd, C. Honerkamp, and W. Hofstetter, Color superfluidity and “baryon” formation in ultracold fermions, Phys. Rev. Lett. **98**, 160405 (2007).
- [66] K. Inaba and S.-i. Suga, Finite-temperature properties of attractive three-component fermionic atoms in optical lattices, Phys. Rev. A **80**, 041602 (2009).
- [67] S. Hoshino and P. Werner, Superconductivity from emerging magnetic moments, Phys. Rev. Lett. **115**, 247001 (2015).
- [68] A. Koga and P. Werner, Superconductivity in the two-band hubbard model, Phys. Rev. B **91**, 085108 (2015).
- [69] K. Ishigaki, J. Nasu, A. Koga, S. Hoshino, and P. Werner, Spontaneously orbital-selective superconductivity in a three-orbital hubbard model, Phys. Rev. B **98**, 235120 (2018).
- [70] Y. Okanami, N. Takemori, and A. Koga, Stability of the superfluid state in three-component fermionic optical lattice systems, Phys. Rev. A **89**, 053622 (2014).
- [71] C. Yue, S. Hoshino, A. Koga, and P. Werner, Unconventional pairing from local orbital fluctuations in strongly correlated A_3C_{60} , Phys. Rev. B **104**, 075107 (2021).
- [72] T. Momoi and K. Kubo, Ferromagnetism in the hubbard model with orbital degeneracy in infinite dimensions, Phys. Rev. B **58**, R567 (1998).
- [73] K. Held and D. Vollhardt, Microscopic conditions favoring itinerant ferromagnetism: Hund’s rule coupling and orbital degeneracy, The European Physical Journal B - Condensed Matter and Complex Systems **5**, 473 (1998).
- [74] H. Yanatori and A. Koga, Finite-temperature phase transitions in the $SU(n)$ hubbard model, Phys. Rev. B **94**, 041110 (2016).
- [75] A. Koga and H. Yanatori, Spontaneously symmetry-breaking states in the attractive $su(n)$ hubbard model, J. Phys. Soc. Jpn. **86**, 034702 (2017).
- [76] H. Georgi, *Lie algebras in particle physics: from isospin to unified theories* (Taylor & Francis, 2000).
- [77] M. Gell-Mann, Symmetries of Baryons and Mesons, Phys. Rev. **125**, 1067 (1962).
- [78] P. Werner, A. Comanac, L. de’ Medici, M. Troyer, and A. J. Millis, Continuous-Time Solver for Quantum Impurity Models, Phys. Rev. Lett. **97**, 076405 (2006).
- [79] A. Koga, J. Bauer, P. Werner, and T. Pruschke, Polarized superfluid state in a three-dimensional fermionic optical lattice, Phys. E: Low-Dimens. Syst. Nanostructures **43**, 697 (2011).
- [80] H. Shinaoka, J. Otsuki, M. Ohzeki, and K. Yoshimi, Compressing Green’s function using intermediate representation between imaginary-time and real-frequency domains, Phys. Rev. B **96**, 035147 (2017).
- [81] N. Chikano, K. Yoshimi, J. Otsuki, and H. Shinaoka, ir-basis: Open-source database and software for intermediate-representation basis functions of imaginary-time Green’s function, Comput. Phys. Commun. **240**, 181 (2019).
- [82] N. Trivedi, R. T. Scalettar, and M. Randeria, Superconductor-insulator transition in a disordered electronic system, Phys. Rev. B **54**, R3756 (1996).
- [83] N.-H. Tong, S.-Q. Shen, and F.-C. Pu, Mott-hubbard transition in infinite dimensions, Phys. Rev. B **64**, 235109 (2001).
- [84] E. G. C. P. van Loon, A. I. Lichtenstein, M. I. Katsnelson, O. Parcollet, and H. Hafermann, Beyond extended dynamical mean-field theory: Dual boson approach to the two-dimensional extended hubbard model, Phys. Rev. B **90**, 235135 (2014).
- [85] D. Goldberger, Y. Fridman, E. Gull, E. Eidelstein, and G. Cohen, Dynamical mean field theory of the bilayer hubbard model with inchworm monte carlo, Phys. Rev. B **109**, 085133 (2024).
- [86] M. A. Cazalilla and A. M. Rey, Ultracold fermi gases with emergent $su(n)$ symmetry, Reports on Progress in Physics **77**, 124401 (2014).
- [87] A. Koga, N. Kawakami, T. M. Rice, and M. Sigrist, Orbital-selective mott transitions in the degenerate hubbard model, Phys. Rev. Lett. **92**, 216402 (2004).
- [88] L. de’ Medici, A. Georges, and S. Biermann, Orbital-selective mott transition in multiband systems: Slave-spin representation and dynamical mean-field theory, Phys. Rev. B **72**, 205124 (2005).
- [89] S. Hoshino and P. Werner, Spontaneous orbital-selective mott transitions and the jahn-teller metal of A_3C_{60} , Phys. Rev. Lett. **118**, 177002 (2017).
- [90] W. S. Bakr, J. I. Gillen, A. Peng, S. Fölling, and M. Greiner, A quantum gas microscope for detecting single atoms in a hubbard-regime optical lattice, Nature **462**, 74 (2009).
- [91] L. W. Cheuk, M. A. Nichols, M. Okan, T. Gersdorf, V. V. Ramasesh, W. S. Bakr, T. Lompe, and M. W. Zwierlein, Quantum-gas microscope for fermionic atoms, Phys. Rev. Lett. **114**, 193001 (2015).
- [92] M. Jarrell, Hubbard model in infinite dimensions: A quantum monte carlo study, Phys. Rev. Lett. **69**, 168 (1992).
- [93] M. Snoek, I. Titvinidze, C. Tóke, K. Byczuk, and W. Hofstetter, Antiferromagnetic order of strongly interacting fermions in a trap: real-space dynamical mean-field analysis, New J. Phys. **10**, 093008 (2008).
- [94] L. Rampon, F. Šimkovic, and M. Ferrero, Magnetic phase diagram of the three-dimensional doped hubbard model, Phys. Rev. Lett. **134**, 066502 (2025).
- [95] M. Snoek, I. Titvinidze, and W. Hofstetter, Canted antiferromagnetic order of imbalanced fermi-fermi mixtures in optical lattices by dynamical mean-field theory, Phys. Rev. B **83**, 054419 (2011).
- [96] A. Sotnikov, M. Snoek, and W. Hofstetter, Magnetic phases of mass- and population-imbalanced ultracold fermionic mixtures in optical lattices, Phys. Rev. A **87**, 053602 (2013).
- [97] S. Ueda, N. Kawakami, and M. Sigrist, Electronic and magnetic properties in strongly correlated heterostructures, Phys. Rev. B **85**, 235112 (2012).
- [98] F. Grandi, A. Amaricci, M. Capone, and M. Fabrizio, Correlation-driven lifshitz transition and orbital order in a two-band hubbard model, Phys. Rev. B **98**, 045105 (2018).
- [99] B. Bauer, L. Carr, H. G. Evertz, A. Feiguin, J. Freire, S. Fuchs, L. Gamper, J. Gukelberger, E. Gull, S. Guertler, *et al.*, The ALPS project release 2.0: open source software for strongly correlated systems, J. Stat. Mech.: Theory Exp. **2011** (05), P05001.